

Evidence for Three- α Breathing Modes Uncovered by Control Neural Network

Zheng Cheng^{1,2}, Mengjiao Lyu^{1,2,*}, Takayuki Myo^{3,4}, Hisashi Horiuchi⁴, Hiroshi Toki⁴, Zhongzhou Ren^{5,6}, Masahiro Isaka⁷, Mengyun Mao^{1,2}, Hiroki Takemoto⁸, Niu Wan⁹, Wenlong You^{1,2}, and Qing Zhao¹⁰

¹College of Physics, Nanjing University of Aeronautics and Astronautics, Nanjing 210016, China

²Key Laboratory of Aerospace Information Materials and Physics (NUAA), MIIT, Nanjing 211106, China

³General Education, Faculty of Engineering, Osaka Institute of Technology, Osaka, Osaka 535-8585, Japan

⁴Research Center for Nuclear Physics (RCNP), Osaka University, Osaka 567-0047, Japan

⁵School of Physics Science and Engineering, Tongji University, Shanghai 200092, China

⁶Key Laboratory of Advanced Micro-Structure Materials, Ministry of Education, Shanghai 200092, China

⁷Hosei University, 2-17-1 Fujimi, Chiyoda-ku, Tokyo 102-8160, Japan

⁸Faculty of Pharmacy, Osaka Medical and Pharmaceutical University, Takatsuki, Osaka 569-1094, Japan

⁹School of Physics and Optoelectronics, South China University of Technology, Guangzhou 510641, China

¹⁰School of Science, Huzhou University, Huzhou 313000, Zhejiang, China

*mengjiao.lyu@nuaa.edu.cn

ABSTRACT

This work introduces a new Control Neural Network (Ctrl.NN) method to uncover evidence of exotic quantum state, *i.e.*, the breathing modes in 3- α resonant states of ^{12}C nucleus. We provide the most precise microscopic description to date for the ^{12}C energy spectrum, identify two new exotic breathing states, and uncover strong evidence that directly connects the recent experimental observations to the breathing modes. The Ctrl.NN method significantly simplifies numerical calculations of quantum systems under multiple constraints and offers a new perspective for solving the nuclear many-body problem.

Introduction

In quantum physics, one of the most interesting objectives is to discover the exotic quantum states, such as the Bose-Einstein condensation that exists in both cold atom and nuclear physics¹, formulation of molecular structures of both atomic nuclei² and pentaquark particles³, and the recent discussions on the breathing-like excitations of nucleons⁴ or α -clusters in the nuclear systems^{5,6}.

For ^{12}C nucleus, very rich phenomena arouse in the nuclear excited states, such as the intriguing formation of stable alpha clusters that constitutes 3- α resonances above the threshold. In particular, the 0_2^+ Hoyle state at resonant energy of 7.65 MeV is identified as an (0S)- α -condensate state, which plays a crucial role in the stellar nucleosynthesis of Carbon and heavier elements⁷. The condensate nature of the Hoyle state could be further revealed by its possible excitation to the exotic “breathing-like” state, where one of the α -clusters in (0S) condensation is excited to the higher (1S)-orbit^{8,9}. Due to this excitation, the breathing state is characterized by a very large radius and a giant isoscalar monopole transition strength to the Hoyle state. The existence of breathing excitation also modifies the temperature dependence of the 3- α reaction rate at $T_9 \gtrsim 2$ ($T_9 = T/10^9$ K) in stars and thus potentially revises the stellar evolution and nucleosynthesis models⁶.

Recently, a rich energy spectrum has been determined experimentally for the resonant states of ^{12}C ^{5,6,10-15}. The 2_2^+ and 4_2^+ states of the Hoyle band are observed at 10.0 MeV^{5,6,10,12} and 13.3 MeV¹³, which are explained as the rotation of a 3- α cluster structure with an equilateral triangle shape based on D_{3h} symmetry¹⁵. However, discussions on the third band of ^{12}C is much more limited. Experimentally, a broad 0^+ resonance is reported at about 10 MeV¹⁰, which is also reproduced by recent *ab initio* calculation with a relatively small radius¹⁶. On the other hand, the isoscalar-strength distribution measured between 8-12 MeV indicates that the broad resonance is composed by two separate 0_3^+ and 0_4^+ states that are located at 9.04 MeV and 10.56 MeV, respectively¹⁰. Theoretically, the 0_3^+ state is interpreted as a breathing-like mode of the Hoyle state⁸, where one of the α -clusters in (0S) condensation is excited to the higher (1S)-orbit, which is named as “breathing state”. Due to this excitation, the breathing state is characterized by a very large radius and its giant isoscalar monopole transition strength to the Hoyle state. In recent experiments, excess monopole strength at $E \approx 9$ MeV has been observed^{5,6}, which support the existence of giant monopole transition between 0_3^+ and 0_2^+ states^{8,9,17}. For the higher J elements, the 2_3^+ state at 11.1 MeV has been

proposed in early experiment¹⁸ and subsequently reexamined in recent work¹⁹. Additionally, there is tentative evidence for a broad 2^+ state between 10.5 and 12 MeV²⁰, which is considered as a candidate of the 2_3^+ state. In previous works, this state has not been yet associated to the breathing states except that it is assigned to the 0_3^+ band in cluster model calculations^{21,22}.

In this work, we propose a new microscopic model of ^{12}C guided by a Control Neural Network (Ctrl.NN) that successfully reproduce the existing experimental spectrum of ^{12}C above the $3\text{-}\alpha$ threshold energy with considerable accuracy. We predict the 2_3^+ and 4_3^+ states as two new breathing states and provide new evidence that connects current experimental spectrum to these breathing modes.

Results

Energy spectrum of ^{12}C

We use the Ctrl.NN to evolve 28 sets of basis wave functions under different multiple constraint conditions, resulting in a total of 840 bases, with each set comprising 30 cluster wave functions. Then, all these bases are angular momentum projected and diagonalized to find the energy spectrum and eigenstates of ^{12}C . The ground state and Hoyle state energies of the ^{12}C nucleus obtained from our calculations are respectively -89.66 MeV and -81.98 MeV, consistent with the values calculated in previous works^{21,22}. Our results indicate the presence of excited 0_3^+ and 0_4^+ states at 9.37 MeV and 11.08 MeV, respectively, which fit very well with the experimental values of 9.04 MeV and 10.56 MeV¹⁰. As a benchmark, we compare our results of the four 0^+ state levels with values from previous works^{8,21,22} in Fig. 1. Additionally, values calculated with a single constraint in the Ctrl.NN method are shown for comparison. We have found that the Ctrl.NN method can reproduce results in previous works such as “THSR1”²¹ and “REM”²², under single radius or energy constraint, respectively. By adopting multi-objective optimization in this study, the 0^+ spectrum shows improved consistency with experimental data compared to the other works.

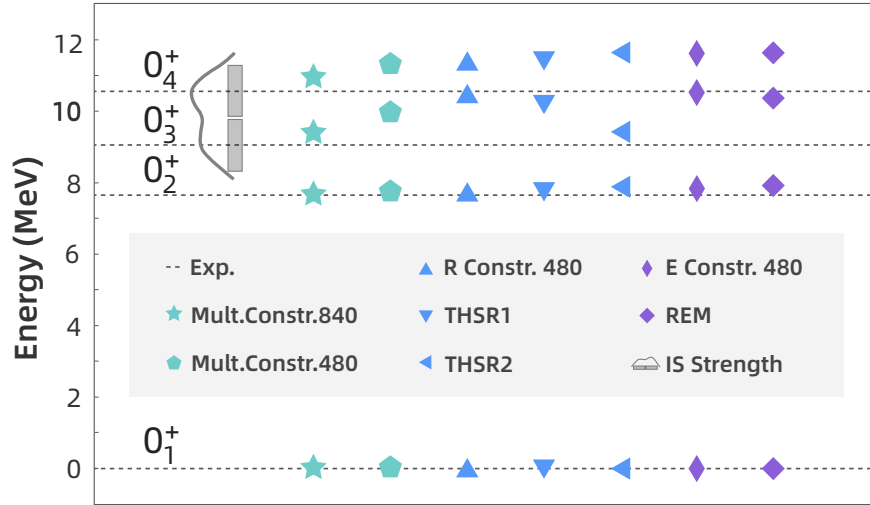


Figure 1. Excitation energies of 0^+ states for ^{12}C measured from the ground state energy. Calculations employing a similar constraint strategy are represented with same color. Different microscopic calculation results by the THSR1²¹, THSR2⁸, REM²² and our Ctrl.NN method with multi- or single-objective optimization are compared with the experimental data^{10,18,23}. The grey curve shows the isoscalar strength distributions from Ref¹⁰.

We further calculate the complete positive parity energy spectrum of ^{12}C by diagonalizing the 840 bases after angular momentum projection, and compare with the available experimental observations¹⁰⁻¹⁵, as shown in Fig.2. It is noteworthy that the spectrum predicted by the Ctrl.NN method is in excellent agreement with the existing experimental data for $3\text{-}\alpha$ resonant states, which has not been achieved by microscopic calculations before. The Hoyle state is successfully reproduced, especially regarding the energy level spacing between the 0_3^+ and 2_3^+ states. In previous works, the Hoyle band has been interpreted as a rotational band characterized by a rigid equilateral triangular intrinsic structure¹⁵. In this work, we have calculated the $B(E2)$ transitions between the energy levels, as shown in Fig. 2, and determined the ratio $B(E2; 4_2^+ \rightarrow 2_2^+)/B(E2; 2_2^+ \rightarrow 0_2^+)$ to be 6.53, which exceeds the value of $10/7$. Therefore, our result supports the non-rigid intrinsic structure in the Hoyle band as already pointed out in Ref.^{21,24}. We also find a large value of $B(E2; 4_2^+ \rightarrow 2_3^+)$ as $1201.9 \text{ e}^2\text{fm}^4$, which shows that the 4_2^+ state has strong configuration mixing with 4_3^+ state. For the next 0_3^+ breathing band, the giant value of $B(E2; 2_3^+ \rightarrow 0_3^+) = 809.2$

$e^2\text{fm}^4$ indicates that the 2_3^+ and 0_3^+ states have remarkably similar structures. In subsequent analysis, we show that they are breathing counterparts of the Hoyle band.

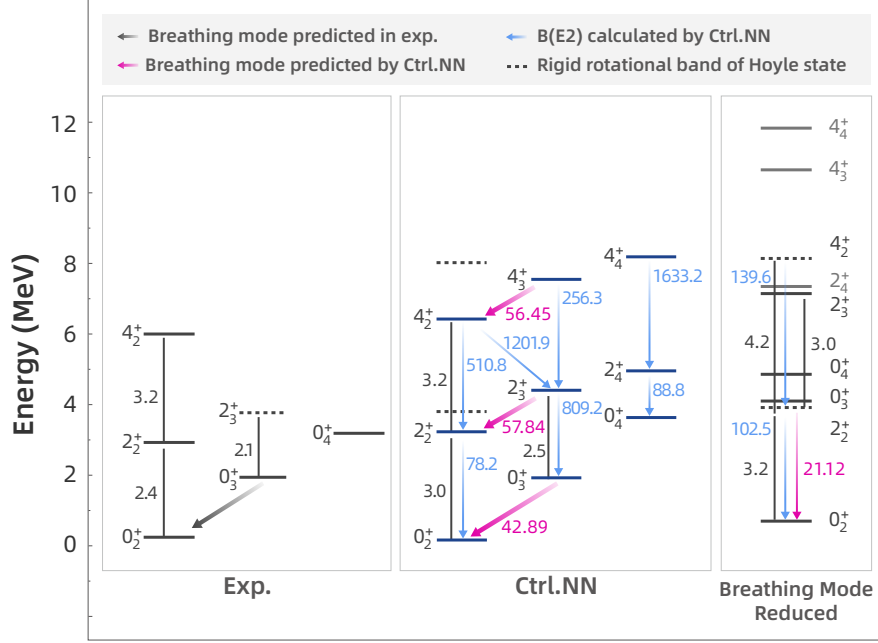


Figure 2. The resonant states energy spectrum of ^{12}C nucleus. The energies were measured from the $3\text{-}\alpha$ threshold energy. The microscopic calculation by Ctrl.NN method are compared with experimental results^{5,6,10–15,18–20,20}. Experimental prediction for the existence of breathing mode in the Hoyle state comes from Refs^{5,6}. Experimental evidence supporting the existence of the 2_3^+ state is provided in Refs.^{18–20}.

New breathing mode of ^{12}C

To explore the new breathing modes of ^{12}C , we calculate the electric monopole transition strengths of the 0^+ , 2^+ and 4^+ states, as shown in Tab 1. Here, the most significant transitions are shown as purple arrows in Fig.2. Consistent with previous

Table 1. The electric monopole transition strengths $M(E0)$ for ^{12}C , including the giant values between the breathing states. All units are in efm^2 .

Transition	$M(E0)$	Transition	$M(E0)$	Transition	$M(E0)$
$0_2^+ \rightarrow 0_1^+$	6.08	$2_2^+ \rightarrow 2_1^+$	5.51	$4_2^+ \rightarrow 4_1^+$	2.24
$0_3^+ \rightarrow 0_1^+$	3.25	$2_3^+ \rightarrow 2_1^+$	4.21	$4_3^+ \rightarrow 4_1^+$	3.33
$0_4^+ \rightarrow 0_1^+$	3.48	$2_4^+ \rightarrow 2_1^+$	0.46	$4_4^+ \rightarrow 4_1^+$	2.97
$0_3^+ \rightarrow 0_2^+$	42.89	$2_3^+ \rightarrow 2_2^+$	57.84	$4_3^+ \rightarrow 4_2^+$	56.45
$0_4^+ \rightarrow 0_2^+$	2.11	$2_4^+ \rightarrow 2_2^+$	2.67	$4_4^+ \rightarrow 4_2^+$	25.34
$0_4^+ \rightarrow 0_3^+$	20.78	$2_4^+ \rightarrow 2_3^+$	1.30	$4_4^+ \rightarrow 4_3^+$	51.43

works, we obtain a giant value for $M(E0; 0_3^+ \rightarrow 0_2^+)$ as 42.89efm^2 , which shows that the 0_3^+ state is indeed the breathing mode of 0_2^+ state. Our prediction for the excitation energy of the 0_3^+ state is 9.45MeV , closely matching the experimental value of $E_x \approx 9 \text{MeV}$, which corresponds to the observation of excess monopole strength^{5,6}. Furthermore, we predict the 2_3^+ state as the breathing mode of 2_2^+ state, with a giant transition strength of $M(E0; 2_3^+ \rightarrow 2_2^+) = 57.84 \text{efm}^2$, which has not yet been discussed in previous works. For the $M(E0; 4_3^+ \rightarrow 4_2^+)$ transition, a large strength of 56.45efm^2 is obtained, but radius difference between 4_3^+ and 4_2^+ states is not significant. Therefore, we consider the 4_3^+ state as the “semi-breathing mode” of 4_2^+ . The giant transition strengths listed above demonstrate the presence of one-to-one correspondence in the breathing modes between the 0_3^+ band and the Hoyle band of $3\text{-}\alpha$ resonances. Thus, we propose to name the 0_3^+ band as “breathing band”.

To provide strong support for the existence of breathing modes in the 3- α resonance, we further scrutinize the substantial contribution to the resonance spectrum made by the breathing states. This is done by artificially reducing the breathing mode in the theoretical model space, where basis sets with large eigenvalues of root-mean-square radii are discarded. Since the breathing states are characterized by their large radii, the monopole transition strengths between the Hoyle band and the breathing band are significantly diminished for the 0^+ , 2^+ , and 4^+ states as 21.12 efm², 25.75 efm², and 14.66 efm², respectively. More details are discussed in Supplementary Note 11. In the reduced model space, the 0_2^+ Hoyle state and the 2_2^+ states exhibit relatively minor increment of excitation energy, as shown in Fig. 2. However, the excitation energies of breathing band states, including the 0_3^+ , 2_3^+ , and 4_3^+ , become significantly higher. Especially, the energy levels of 0_3^+ and 2_3^+ states show clear deviation from the experimental values. The findings indicate that the reduction of the breathing mode results in a substantial discrepancy between the theoretically energy spectrum and the experimental observations. In contrast, the remarkable consistency observed in the full calculation indicates that current experimental observations strongly support the existence of breathing modes in the 3- α resonance.

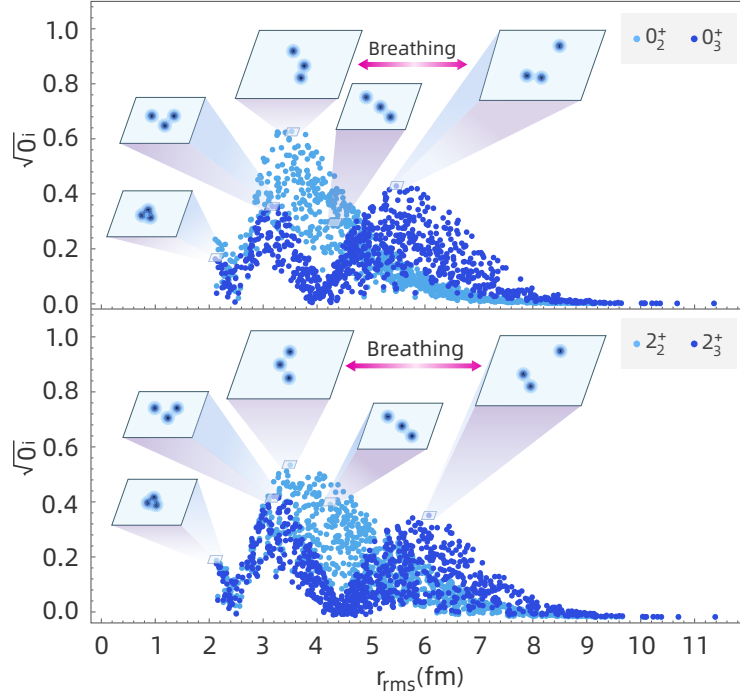


Figure 3. Configuration distribution of 0_2^+ , 0_3^+ , 2_2^+ and 2_3^+ states. O_i represents the amplitude. r_{rms} represents the root-mean-square radius of each basis.

To understand the formation of breathing states, we analyze the contribution from bases with different configurations to the resonant states. Here, O_i is defined as the squared overlap (from supplementary material Eq.(32)) between each basis and the total wave function. We plot the distribution of $\sqrt{O_i}$ with respect to the root-mean-square radius r_{rms} in Fig. 3, for the 0^+ and 2^+ breathing modes. It is shown that for breathing states 0_3^+ and 0_2^+ , $\sqrt{O_i}$ has a significant distribution over a broad model space, covering a range of approximately 2–8 fm, which suggests that the bases generated by the Ctrl.NN provide a very efficient model space for the description of giant resonant states of ^{12}C . It is found that the darkblue peak at 6 fm of $^8\text{Be}+^4\text{He}$ configuration plays a key role in the formation of the breathing state, as it has a large electric monopole transition strengths to the lightblue peak at 3.5 fm, which corresponds to obtuse configurations that contribute most to the 0_2^+ and 2_2^+ states in the Hoyle band, as shown by the arrows in Fig. 3. More detailed information is provided in the Supplementary Note 7–10.

Discussion

In this work, we proposed and performed the microscopic calculations of ^{12}C , guided by a Control Neural Network (Ctrl.NN) to uncover the exotic breathing modes in 3- α resonant states. By imposing multiple constraints on the many-body wave function via Ctrl.NN, we successfully reproduced the existing experimental spectrum of ^{12}C above the 3- α threshold with considerable

accuracy, providing a solid foundation for further analyses. The rotational band of the Hoyle state was found to be non-rigid by examining the band level positions and B(E2) transitions. The breathing modes between the 0_3^+ and 0_2^+ states were confirmed through significant monopole transition. Two new breathing modes, *i.e.*, the transitions between 2_3^+ and 2_2^+ states and between 4_3^+ and 4_2^+ states, were revealed. Artificially reducing the breathing mode in the theoretical model led to significant deviations in the energy spectrum prediction for ^{12}C from the experimental values. In contrast, the remarkable consistency observed in the full calculation indicated that current experimental observations strongly support the existence of breathing modes in the $3-\alpha$ resonance. This research had been made feasible by the merits of the new Ctrl.NN method, which significantly simplifies numerical calculations under multiple constraints and offers a new perspective for solving the nuclear many-body problem.

Method

Control Neural Network Method

The $3-\alpha$ resonant states usually exhibit a giant spatial distribution which lead to significant difficulties for microscopic theories. In recent works, constraint conditions for radius^{8,9,24,25}, energy^{22,26–28}, or deformation^{29–32} are usually imposed to limit the model space, and used independently as formulated in different algorithms. However, the interplay between the geometric properties, *e.g.* radius and rotational symmetry, and the dynamical quantities including the energy surface and derivatives, is essential for the formulation of $3-\alpha$ resonance. Hence, for a proper treatment, all these constraints for the resonance wave functions should be simultaneously involved. Here, we propose a Control Neural Network (Ctrl.NN) which accepts parameters in the microscopic wave function as input and learns from multiple constraint conditions with high efficiency in the evolution of quantum state. Hence we can obtain the trained Ctrl.NN which is capable to generate proper microscopic wave functions for further calculation. This neural network allows general applications for quantum many-body problems by substituting the wave functions and the constraint targets.

In this work for the $3-\alpha$ resonance, we impose multiple constraints according to the physical properties of the resonant states which are satisfied by guiding the evolution of cluster wave function via the Ctrl.NN. These include the spatial extension, rotational symmetry, and energy variation of the cluster resonant states. In supplementary material, we also show two other applications of control neural networks for solving quantum many-body problems in both nuclear physics and condensed matter physics. For energy variational problem, the multiple cooling method³³, which can significantly improve the calculations of the ground and excited states of light atomic nuclei, can be guided by the Ctrl.NN, such as explained in Sec.II of the supplementary material for calculations of ^{8-10}Be nuclei. We also show in Sec. IV of the supplementary material how the Ctrl.NN can be used to construct cat states targeting at high precision fidelity and defect density under time boundary conditions for Ising model on 24, 50, and 100 lattices.

Here, we explain the fundamental concepts of the Ctrl.NN, with the network structure shown in Fig. 4. The more technical explanations with detailed formulation can be found in Supplementary Note 3. For the $3-\alpha$ resonant states, we adopt the microscopic cluster wave functions which explicitly treat antisymmetrization of 12 nucleons. Similar approach are widely used in recent researches for $5-\alpha$ systems²⁵. The detailed introduction of cluster wave function and effective Hamiltonian can be found in Supplementary Note 1. The total intrinsic wave function of the $3-\alpha$ system is a superposition of the basis wave functions as

$$|\Psi\rangle = \sum_{i=1}^m C_i \mathcal{A} \{ \Phi_\alpha(Z_1^{(i)}) \Phi_\alpha(Z_2^{(i)}) \Phi_\alpha(Z_3^{(i)}) \}. \quad (1)$$

Here, C_i is coefficient yielded by the diagonalization, and Φ_α is the microscopic α -cluster wave function. The m is the number of bases in superposition. The $Z_1^{(i)}, Z_2^{(i)}, Z_3^{(i)}$ are generated coordinates of α clusters, and we denote them as a set $\{Z^{(i)}\} = Z_1^{(i)}, Z_2^{(i)}, Z_3^{(i)}$. In order to restore the rotational symmetry, the total wave function can be obtain after angular momentum projection technique $\hat{P}_{KM}^J |\Psi\rangle$ (See Supplementary Note 3 for more details). The input X of the neural network is expressed as (See Supplementary Note 2)

$$X(\{Z\}) = \left[\{Z^{(1)}\}, \dots, \{Z^{(m)}\}, E(\{Z\}) \right]^T, \quad (2)$$

where the intrinsic energy $E(\{Z\})$ of the $3-\alpha$ system is obtained diagonalizing the present basis set in the intrinsic frame³³.

The output is the amount of change in coordinates $\{\Delta Z^{(i)}\}$, which is used to form the the new input $X(\{Z'\})$ in the next iteration. All values in the input, output, and hidden layers are complex numbers. With just-in-time training, this neural network will gradually optimize the basis set by predicting the proper coordinate changes to satisfy the three constraints imposed to the cluster wave function. In Fig.5, the constrained evolution of basis set demonstrated, where various three- α configurations emerge from the randomly generated initial states. Detailed discussion for each configuration can be found in Supplementary Note 5.

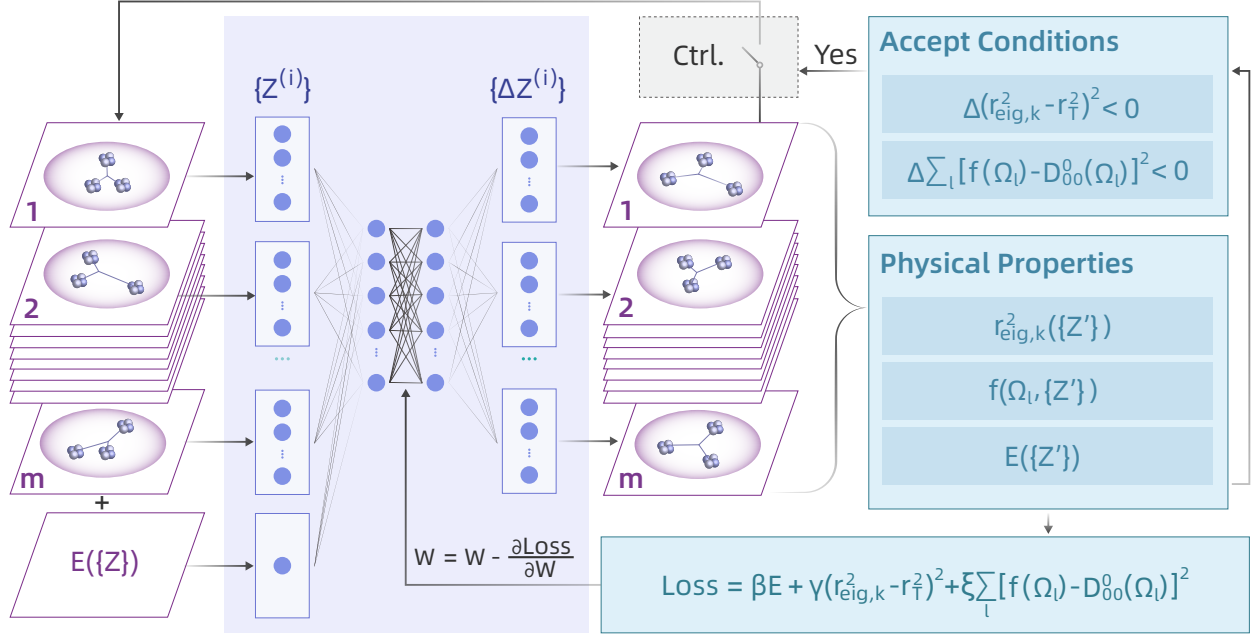


Figure 4. The structures of Control Neural Network. The small slateblue circles symbolize the complex nodes of the neural network. The violet modules denote the input and output units. The turquoise modules denote the physical quantities and algorithms, as introduced in the main text. The update of input is controlled by turning on or off the “Ctrl.” switch.

Multiple constraints

In each iteration, a new basis set $\{Z'\}$ is obtained and diagonalized to yield the new total intrinsic wave function $\Psi(\{Z'\})$ and physical properties corresponding to each of the three constraints, including $E(\{Z'\})$, $r_{\text{eig},k}^2(\{Z'\})$ and $f(\Omega_l)$. Here, $E(\{Z'\})$ is the minimum eigenvalue of the Hamiltonian matrix H with respect to the new basis set, $r_{\text{eig},k}^2$ is the k -th eigenvalue of mean-square radius obtained by diagonalizing the matrix $[\langle \Psi(\{Z^{(i)'}\}) | \hat{R}^2 | \Psi(\{Z^{(j)'}\}) \rangle]_{m \times m}$, and $f(\Omega_l, \{Z'\}) = \langle \Psi(\{Z'\}) | \hat{R}(\Omega_l) | \Psi(\{Z'\}) \rangle$ is a measure of rotational symmetry through the overlap between the original total intrinsic wave function $\Psi(\{Z'\})$ and the one rotated by the l -th Euler angle Ω_l . The three properties calculated from the output are constrained for the total intrinsic wave function by training the neural network with the loss function formulated as

$$\text{Loss} = \beta E + \gamma (r_{\text{eig},k}^2 - r_T^2)^2 + \xi \sum_{l=1}^L [f(\Omega_l) - D_{MK}^J(\Omega_l)]^2, \quad (3)$$

where β , γ , and ξ are the weight parameters of this three items, with ratio $\beta : \gamma : \xi = 1 : 4 : 2$. The first term E introduces energy variation, which reduces the lowest energy with respect to the basis set, and thus to avoid unphysical states that satisfies only the other two constraint conditions. The second term $(r_{\text{eig},k}^2 - r_T^2)^2$ is used to constrain the spatial extension of nuclear wave function to a target value r_T^2 . This condition is an improved one from the previous works which selected the eigenstates with eigenvalues smaller than a cut value R_{cut} for inclusion in the model space^{8,17}. In this work, we propose constraining the 2nd to 4th eigenvalues of the mean-square radius to various target values. This approach allows the corresponding eigenstates, which have fewer nodal structures, to evolve into states with a relatively larger radius. This ensures effective coverage of the model space for the resonance states with substantial spatial extension. The third term $[f(\Omega_l) - D_{MK}^J(\Omega_l)]^2$ constrains the rotational symmetry of the wave function under rotations, where the Wigner function $D_{MK}^J(\Omega_l)$ is the target value derived for the eigenstates of angular momentum J with $J_z = M$ or K for bra and ket, respectively³⁴. Using this constraint, the rotational symmetry is taken into account for the nuclear resonance states in the intrinsic frame before angular momentum projection, and thus to limit the model space of the wave function in evolution. The restoration of this rotational symmetry is discussed in more detail through plotting of the density distributions (in Supplementary Note 5).

The merit of the present loss function is the interplay between different constraints, which collectively limit the model space of many-body wave function into an essential subset in the evolution, thereby providing the most accurate description

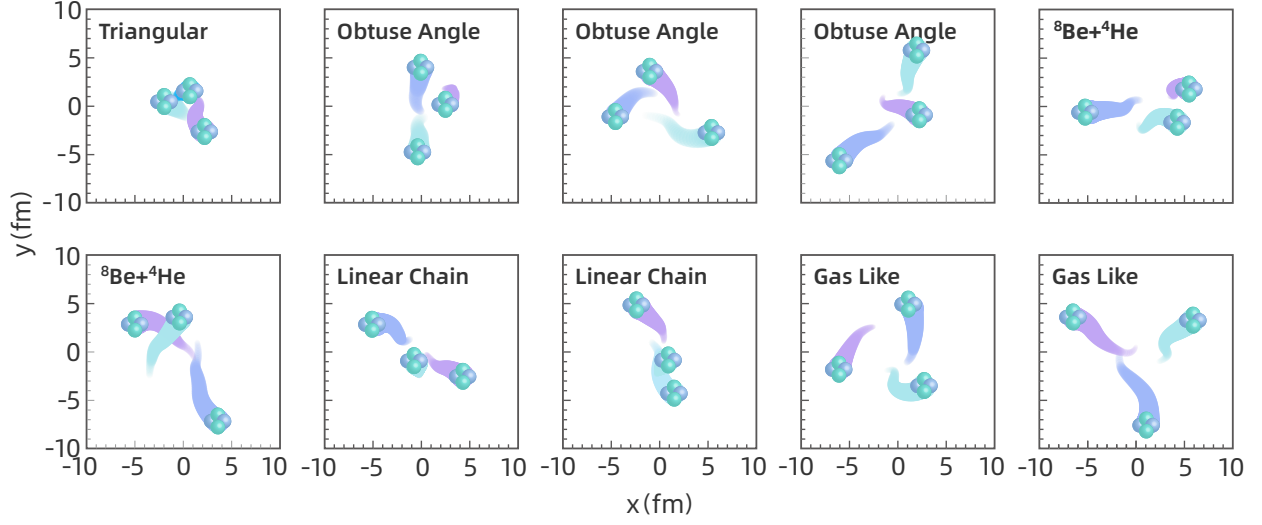


Figure 5. The constrained evolution of basis set guided by the Ctrl.NN. Various three- α configurations emerge from the randomly generated initial states. Configurations shown in this figure are selected from a set of 30 bases after evolution. The multiple constraints are introduced in Eq.1 in the main text, where $r_T^2 = 13 \text{ fm}^2$, and $J = M = K = 0$. (A Movie demonstrating Ctrl.NN guided basis set evolution could be found in Supplementary Movie 1.

of the physical states after iterations. To speed up the convergence of wave function evolution, we adopt control conditions for accepting new inputs from the previous iteration as shown in Fig.4, where we discard the basis sets that deteriorate the constraints to the target radius or rotational symmetry.

Constraint on squared matter radius eigenvalues

In this section, we explain the constraint for squared matter radius eigenvalues introduced as the second term $(r_{\text{eig},k}^2 - r_T^2)^2$ in Loss function. We prepare 28 sets of basis wave functions, each composed of 30 cluster wave functions, and impose different control targets for the 2nd ($k = 2$), 3rd ($k = 3$), and 4th ($k = 4$) eigenvalues of the R^2 matrix, where

$$R_{ij}^2 = \langle \Psi(\{Z^{(i)}\}) | \hat{R}^2 | \Psi(\{Z^{(j)}\}) \rangle. \quad (4)$$

Under this constraint, we evolve each set of bases to a target r_k^2 eigenvalue, and thus prepare a sub model space with proper spatial scale. Especially, the first few eigenstates of r_k^2 has only small number of nodes, which ensures effective coverage for the low-lying 0_{1-4}^+ states. As shown in Supplementary note 5, the largest targets are 8 fm^2 , 16 fm^2 , and 19 fm^2 for $r_{\text{eig},2-4}^2$, respectively. We note that this constraint is not used independently, but imposed simultaneously with the energy and rotational symmetry constraints.

Treatment of resonant states

In this work, the Hoyle band and the 0_3^+ band are all resonant states located above the $\alpha + \alpha + \alpha$ threshold. Resonant states are time-dependent states which do not break up immediately so that they can be treated numerically as stationary solutions of the Schrödinger equation with boundary conditions of the outgoing waves. Rigorous solutions to such problems could be obtained by non-Hermitian quantum mechanics such as complex scaling methods (CSM)^{35,36}. In the bound state approximation^{8,17,21,22,25}, the outgoing waves are replaced by square-integrable waves obtained using variational approach, and validity of the approximation are verified by correct descriptions of the energy spectra. In the study of the resonant state of the ^{12}C nucleus, a large number of bases with different configurations are often superposed to cover the entire model space, making it difficult to avoid contamination from the continuum states, especially when the bases of giant radii are taken into account. However, a strict constraint for the radius may lead to insufficient model space which can not reproduce correct energy spectrum. In our study, we demonstrate that this contradiction is resolved through the imposition of multiple constraints, whereby the eigenvalues of the squared matter radius are relatively small ($r_{\text{eig}} \leq 5 \text{ fm}$), yet the experimental spectrum is accurately reproduced. Another evidence is the zero contribution to the total wave functions from the large radius bases. For

example, in the $\sqrt{O_i-r_{\text{rms}}}$ distribution as shown in Fig. 3, it is found that 840 bases cover a broad model space with radius range of approximately 10 fm, but the overlap between total wave function and the bases with radius $r_{\text{rms}} > 8$ fm vanishes. As the large radius bases are essential for the existence continuum states, this distribution shows that the contamination from continuum is avoided to the largest extent.

Data availability

All data relevant to this study are shown in the paper and its Supplementary file, and more details are available from the corresponding authors.

Code availability

Inquiries about the code in this work will be responded to by the corresponding authors.

References

1. Tohsaki, A., Horiuchi, H., Schuck, P. & Röpke, G. Alpha cluster condensation in ^{12}C and ^{16}O . *Phys. Rev. Lett.* **87**, 192501, DOI: [10.1103/PhysRevLett.87.192501](https://doi.org/10.1103/PhysRevLett.87.192501) (2001).
2. Li, P. J. *et al.* Validation of the ^{10}Be ground-state molecular structure using $^{10}\text{Be}(p, p\alpha)^6\text{He}$ triple differential reaction cross-section measurements. *Phys. Rev. Lett.* **131**, 212501, DOI: [10.1103/PhysRevLett.131.212501](https://doi.org/10.1103/PhysRevLett.131.212501) (2023).
3. Aaij, R., Abellán Beteta, C., Adeva, B. *et al.* Observation of a narrow pentaquark state, $P_c(4312)^+$, and of the two-peak structure of the $P_c(4450)^+$. *Phys. Rev. Lett.* **122**, 222001, DOI: [10.1103/PhysRevLett.122.222001](https://doi.org/10.1103/PhysRevLett.122.222001) (2019).
4. Michel, N., Nazarewicz, W. & Płoszajczak, M. Description of the proton-decaying 0_2^+ resonance of the α particle. *Phys. Rev. Lett.* **131**, 242502, DOI: [10.1103/PhysRevLett.131.242502](https://doi.org/10.1103/PhysRevLett.131.242502) (2023).
5. Li, K. C. W. *et al.* Multiprobe study of excited states in ^{12}C : Disentangling the sources of monopole strength between the energy of the hoyle state and $E_x = 13\text{MeV}$. *Phys. Rev. C* **105**, 024308, DOI: [10.1103/PhysRevC.105.024308](https://doi.org/10.1103/PhysRevC.105.024308) (2022).
6. Li, K. C. W. *et al.* Investigating the predicted breathing-mode excitation of the hoyle state. *Phys. Lett. B* **827**, 136928, DOI: [10.1016/j.physletb.2022.136928](https://doi.org/10.1016/j.physletb.2022.136928) (2022).
7. Hoyle, F. On nuclear reactions occurring in very hot stars. i. the synthesis of elements from carbon to nickel. *Astrophys. J. Suppl.* **1**, 121, DOI: [10.1086/190005](https://doi.org/10.1086/190005) (1954).
8. Zhou, B., Tohsaki, A., Horiuchi, H. & Ren, Z. Breathing-like excited state of the hoyle state in ^{12}C . *Phys. Rev. C* **94**, 044319, DOI: [10.1103/PhysRevC.94.044319](https://doi.org/10.1103/PhysRevC.94.044319) (2016).
9. Takemoto, H. *et al.* Appearance of the hoyle state and its breathing mode in ^{12}C despite strong short-range repulsion of the nucleon-nucleon potential. *Phys. Rev. C* **107**, 044304, DOI: [10.1103/PhysRevC.107.044304](https://doi.org/10.1103/PhysRevC.107.044304) (2023).
10. Itoh, M. *et al.* Candidate for the 2^+ excited hoyle state at $E_x \sim 10\text{MeV}$ in ^{12}C . *Phys. Rev. C* **84**, 054308, DOI: [10.1103/PhysRevC.84.054308](https://doi.org/10.1103/PhysRevC.84.054308) (2011).
11. Itoh, M. *et al.* Nature of 10 MeV state in ^{12}C . vol. 436, 012006, DOI: [10.1088/1742-6596/436/1/012006/meta](https://doi.org/10.1088/1742-6596/436/1/012006/meta) (IOP Publishing, 2013).
12. Zimmerman, W. R. *et al.* Unambiguous identification of the second 2^+ state in ^{12}C and the structure of the hoyle state. *Phys. Rev. Lett.* **110**, 152502, DOI: [10.1103/PhysRevLett.110.152502](https://doi.org/10.1103/PhysRevLett.110.152502) (2013).
13. Freer, M. *et al.* Evidence for a new ^{12}C state at 13.3 MeV. *Phys. Rev. C* **83**, 034314, DOI: [10.1103/PhysRevC.83.034314](https://doi.org/10.1103/PhysRevC.83.034314) (2011).
14. Freer, M. *et al.* Consistent analysis of the 2^+ excitation of the ^{12}C hoyle state populated in proton and α -particle inelastic scattering. *Phys. Rev. C* **86**, 034320, DOI: [10.1103/PhysRevC.86.034320](https://doi.org/10.1103/PhysRevC.86.034320) (2012).
15. Marín-Lámbarri, D. J. *et al.* Evidence for triangular D_{3h} symmetry in ^{12}C . *Phys. Rev. Lett.* **113**, 012502, DOI: [10.1103/PhysRevLett.113.012502](https://doi.org/10.1103/PhysRevLett.113.012502) (2014).
16. Shen, S. *et al.* Emergent geometry and duality in the carbon nucleus. *Nat. Commun.* **14**, 2777, DOI: [10.1038/s41467-023-38391-y](https://doi.org/10.1038/s41467-023-38391-y) (2023).
17. Funaki, Y. Monopole excitation of the hoyle state and linear-chain state in ^{12}C . *Phys. Rev. C* **94**, 024344, DOI: [10.1103/PhysRevC.94.024344](https://doi.org/10.1103/PhysRevC.94.024344) (2016).

18. Ajzenberg-Selove, F. Energy levels of light nuclei $A = 11$ and 12 . *Nucl. Phys. A* **506**, 1–158, DOI: [10.1016/0375-9474\(90\)90271-M](https://doi.org/10.1016/0375-9474(90)90271-M) (1990).
19. Freer, M. *et al.* Reexamination of the excited states of ^{12}C . *Phys. Rev. C* **76**, 034320, DOI: [10.1103/PhysRevC.76.034320](https://doi.org/10.1103/PhysRevC.76.034320) (2007).
20. Hyldegaard, S. *et al.* r -matrix analysis of the β decays of ^{12}N and ^{12}B . *Phys. Rev. C* **81**, 024303, DOI: [10.1103/PhysRevC.81.024303](https://doi.org/10.1103/PhysRevC.81.024303) (2010).
21. Funaki, Y. Hoyle band and α condensation in ^{12}C . *Phys. Rev. C* **92**, 021302, DOI: [10.1103/PhysRevC.92.021302](https://doi.org/10.1103/PhysRevC.92.021302) (2015).
22. Imai, R., Tada, T. & Kimura, M. Real-time evolution method and its application to the 3α cluster system. *Phys. Rev. C* **99**, 064327, DOI: [10.1103/PhysRevC.99.064327](https://doi.org/10.1103/PhysRevC.99.064327) (2019).
23. Freer, M. & Fynbo, H. O. U. The hoyle state in ^{12}C . *Prog. Part. Nucl. Phys.* **78**, 1–23, DOI: [10.1016/j.pnpnp.2014.06.001](https://doi.org/10.1016/j.pnpnp.2014.06.001) (2014).
24. Funaki, Y., Horiuchi, H. & Tohsaki, A. Cluster models from rgm to alpha condensation and beyond. *Prog. Part. Nucl. Phys.* **82**, 78–132, DOI: [10.1016/j.pnpnp.2015.01.001](https://doi.org/10.1016/j.pnpnp.2015.01.001) (2015).
25. Zhou, B. *et al.* The 5α condensate state in ^{20}Ne . *Nat. Commun.* **14**, 8206, DOI: [10.1038/s41467-023-43816-9](https://doi.org/10.1038/s41467-023-43816-9) (2023).
26. Zhou, B., Kimura, M., Zhao, Q. & Shin, S.-h. Microscopic calculations for Be isotopes within real-time evolution method. *Eur. Phys. J. A* **56**, 298, DOI: [10.1140/epja/s10050-020-00306-6](https://doi.org/10.1140/epja/s10050-020-00306-6) (2020).
27. Shin, S., Zhou, B. & Kimura, M. Shape of ^{13}C studied by the real-time evolution method. *Phys. Rev. C* **103**, 054313, DOI: [10.1103/PhysRevC.103.054313](https://doi.org/10.1103/PhysRevC.103.054313) (2021).
28. Zhao, Q., Zhou, B., Kimura, M., Motoki, H. & Shin, S.-h. Microscopic calculations of ^6He and ^6Li with real-time evolution method. *Eur. Phys. J. A* **58**, 25, DOI: [10.1140/epja/s10050-021-00648-9](https://doi.org/10.1140/epja/s10050-021-00648-9) (2022).
29. Suhara, T. & Kanada-En'yo, Y. Quadrupole deformation β and γ constraint in a framework of antisymmetrized molecular dynamics. *Prog. Theor. Phys.* **123**, 303–325, DOI: [10.1143/PTP.123.303](https://doi.org/10.1143/PTP.123.303) (2010).
30. Kanada-En'yo, Y., Kimura, M. & Ono, A. Antisymmetrized molecular dynamics and its applications to cluster phenomena. *Prog. Theor. Exp. Phys.* **2012**, 01A202, DOI: [10.1093/ptep/pts001](https://doi.org/10.1093/ptep/pts001) (2012).
31. Suhara, T. & Kanada-En'yo, Y. Cluster structures in ^{11}B . *Phys. Rev. C* **85**, 054320, DOI: [10.1103/PhysRevC.85.054320](https://doi.org/10.1103/PhysRevC.85.054320) (2012).
32. Kobayashi, F. & Kanada-En'yo, Y. Novel cluster states in ^{10}Be . *Phys. Rev. C* **86**, 064303, DOI: [10.1103/PhysRevC.86.064303](https://doi.org/10.1103/PhysRevC.86.064303) (2012).
33. Myo, T. *et al.* Variation of multi-slater determinants in antisymmetrized molecular dynamics and its application to ^{10}Be with various clustering. *Phys. Rev. C* **108**, 064314, DOI: [10.1103/PhysRevC.108.064314](https://doi.org/10.1103/PhysRevC.108.064314) (2023).
34. Horiuchi, H. & Ikeda, K. Cluster model of the nucleus. *Clust. models other topics* DOI: [10.1142/97898144415453_0001](https://doi.org/10.1142/97898144415453_0001) (1986).
35. Moiseyev, N. *Non-Hermitian quantum mechanics* (Cambridge University Press, 2011).
36. Myo, T., Kikuchi, Y., Masui, H. & Katō, K. Recent development of complex scaling method for many-body resonances and continua in light nuclei. *Prog. Part. Nucl. Phys.* **79**, 1–56, DOI: [10.1016/j.pnpnp.2014.08.001](https://doi.org/10.1016/j.pnpnp.2014.08.001) (2014).

Acknowledgements

This work is supported by the National Natural Science Foundation of China (Grants No. 12105141, No. 12035011, No. 11975167), by the National Key R&D Program of China (Contract No. 2023YFA1606503), by the Jiangsu Provincial Natural Science Foundation (Grants No. BK20210277), by the 2021 Jiangsu Shuangchuang (Mass Innovation and Entrepreneurship) Talent Program (Grants No. JSSCBS20210169), by the National Undergraduate Training Program for Innovation and Entrepreneurship (Grants No. 202110287149Y), by the JSPS KAKENHI Grant No. JP22K03643, and by the JST ERATO Grant No. JPMJER2304, Japan.

Author contributions

Z.C. and M.L. proposed the idea of Control Neural Network and formulated the mathematical framework. T.M. proposed the idea of Multiple Cooling for superposed microscopic wave function of atomic nuclei. H.H. proposed the idea of investigation of breathing states. Z.C. performed the coding work and numerical calculation. T.M. and Q.Z. provided important help in

formulating the constraint algorithms. M.M. and W.Y. proposed and performed applications of Ctrl.NN into the condensed matter physics in supplementary material. Z.C. and M.L. prepared the manuscript. T.M., H.H., H.T., Z.R., M.I., H.T., N.W., W.Y., and Q.Z. contributed to the discussion of results and were involved in revising the manuscript.

Competing interests

The authors declare no competing interests.

Additional information